Nanoscale

Accepted Manuscript

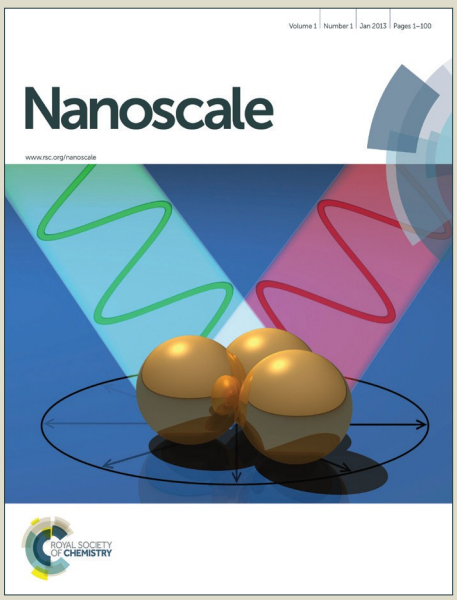

ROYAL SOCIETY OF CHEMISTRY

www.rsc.org/nanoscale

Journal Name

ARTICLE

Thiazole Derivative-Modified Upconversion Nanoparticles for Hg^{2+} Detection in Living Cells

Received 00th January 20xx,
Accepted 00th January 20xx

DOI: 10.1039/x0xx00000x

www.rsc.org/

Bin Gu,[a] Yi Zhou,[a] Xiao Zhang,[a] Xiaowang Liu,[b] Yuhai Zhang,[b] Robert Marks,[d] Hua Zhang,[a] Xiaogang Liu[b] and Qichun Zhang*[a,c]

Mercury ion (Hg^{2+}) is an extremely toxic ion, which will accumulate in human bodies and cause severe nervous system damage. Therefore, the sensitive and efficient monitoring of Hg^{2+} in human bodies is of great importance. Upconversion nanoparticles (UCNP) based nano probes exhibit no autofluorescence, deep penetration depth and chemical stability in biological samples, as well as a large anti-Stokes shift. In this study, we developed a thiazole-derivative-functionalized UCNPs, and employed upconversion emission intensity ratio of 540 nm to 803 nm (I_{540}/I_{803}) as a ratiometric signal to detect Hg^{2+} in living cells and showed excellent photo stability and high selectivity. Our nano probe was characterized by transmission electron microscopy (TEM) and powder X-ray diffraction (PXRD). The low cytotoxicity of our probe was confirmed by an MTT assay and the UCL test in Hela cells was carried out by confocal microscopy. Our results demonstrated that organic-dye-functionalized UCNPs should be a good strategy to detect toxic metal ions when studying cellular biosystems.

Introduction

Detection of the structural and functional properties in living systems is a perennial key challenge for a long time.[1-8] For instance, diagnosis and treatment of cancer necessitate highly contrasted real-time bioimaging.[9-11] Conventional luminescent materials such as organic dyes and quantum dots[12] (QDs) have been explored in the past decades. However, these biolabels have some limitations. Usually the emission lifetimes of organic dyes are short (less than 100 ns),[13] which are difficult to differentiated from other short-lived autofluorescence from biological samples. The QD has high toxicity and short circulation half time,[14] which will limit its bioapplication. Therefore, lanthanide doped upconversion nanoparticles (UCNP) have been suggested as a promising biolabel.

Usually the energy of fluorescent photons are higher than that of excitation ones. However, lanthanide-doped UCNPs can convert near-infrared (NIR) excitation into visible emission of different colors,[15-17] with a large anti-stokes shift of hundreds nanometers.[18-20] UCNPs have many benefits such as chemical stability,[21, 22] non-autofluorescence from biological samples,[21-25] remarkable light penetration depth,[23, 26-28] long lifetime (millisecond time scale)[19, 29] and less damage to samples,[30] thus it can replace conventional organic dyes or quantum dots and has evoked considerable interest for biological applications.

As molecular or ionic probes, UCNPs should combine with other chromophores through luminescence resonance energy transfer (LRET) process. In a LRET system, UCNPs (donor) can transfer the energy to chromophores (acceptor), which will result the change of upconversion luminescence (UCL). Nowadays, several LRET-based sensing and imaging systems have been reported. Li and co-workers developed a cyanine-modified UCNP for the detection of methylmercury;[35] Liu and co-workers discovered manganese dioxide-loaded nanosheets for glutathione detection;[36] Chang and co-workers created a dye-assembled UCNP for sensing zinc ion *in vitro* and *in vivo*.[3] Chen and co-workers used a sensitive time-resolved bioprobe to detect avidin through lanthanide-doped zirconia nanoparticles.[38] Liu and co-worker demonstrated a $NaYF_4$ sandwich structure for calcium ion detection[39] and silver nanoclusters modified UCNP for biothiols detection.[40] This year Qu and co-workers designed a hyaluronic acid modified UCNP for reactive oxygen species detection and bioimaging.[41] Our group also reported the progress to detect hydrogen peroxide,[42] hypochlorous acid[43] and hydrogen sulfide[30] in living cells. Continuing on our research in this direction, we hope to employ our method to detect mercury ion in biosystem because mercury ion, a strong neurotoxin, accumulates in human bodies and cause severe nervous system damage.[44] In the present study we designed and fabricated an inorganic-organic hybrid probe for the detection of mercury ion. The a

[a] School of Materials Science and Engineering Nanyang Technological University, 50 Nanyang Avenue, Singapore 639798. E-mail: qczhang@ntu.edu.sg
[b] Department of Chemistry, National University of Singapore, 3 Science Drive 3, Singapore 117543.
[c] Division of Chemistry and Biological Chemistry, School of Physical and Mathematical Sciences, Nanyang Technological University, Singapore 637371.
[d] Department of Biotechnology Engineering, Ben Gurion University of the Negev, Beer Sheva, Israel, 8410501

‡ Electronic Supplementary Information (ESI) available: NMR, MADLI-TOF MS spectra, *etc*. See DOI: 10.1039/x0xx00000x

Journal Name

ARTICLE

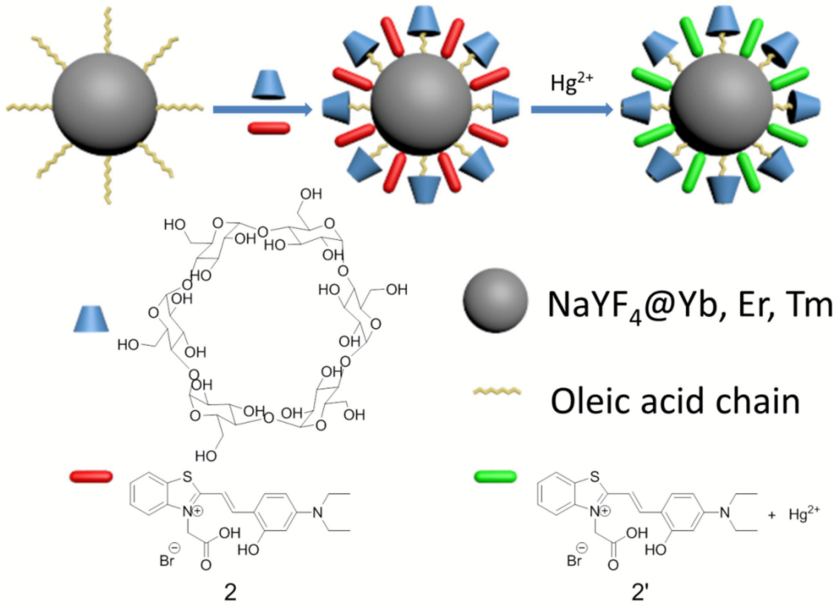

Scheme 1. Schematic illustration of the structure design and proposed mechanism of Hg^{2+} detection.

prepared nanoprobe has excellent biological applications based on the LRET system that is composed of nanophosphors ($NaYF_4$: 20% Yb, 1.8% Er, 0.5% Tm) and a Hg^{2+}-responsive thiazole derivative dye (Scheme 1). We chose hexagonal $NaYF_4$ because of its higher upconversion efficiency, compared with its cubic counterpart.[45] Using the ratio of UCL intensity at 540 nm to 803 nm (I_{540}/I_{803}) as the detection signal, we also demonstrated that the intensity of 540 nm would recover gradually with the increased amount of Hg^{2+}. Moreover, the as-prepared UCNPs could monitor Hg^{2+} in living cells.

Results and Discussion

Design Principle of the Hg^{2+} Probe

Our design strategy was based on the fact that UCNP could

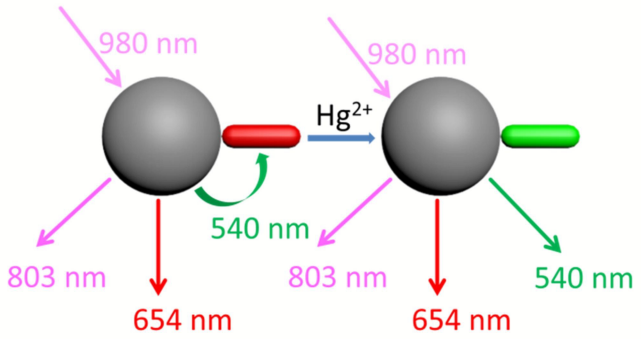

Scheme 2. Schematic illustration of the LRET process from UCNP to compound **2**.

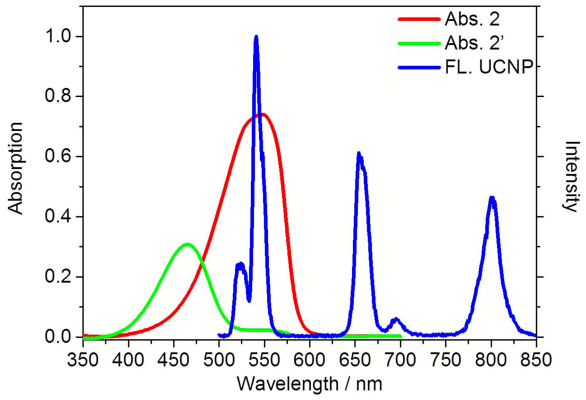

Fig. 1. UV-Vis absorption (red and green) of compound **2** and 2' and upconversion emission (blue) of OA-UCNP.

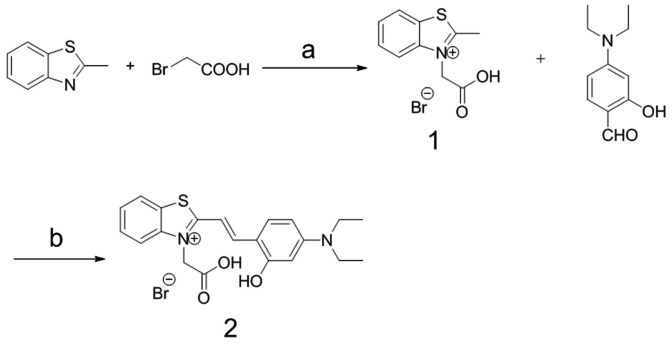

Scheme 3. The synthesis route of compound **2**. Reagents and conditions: (a) toluene, reflux, 20h; (b) piperidine/ethanol, reflux, 24h.

transfer energy to the chromophore by LRET process (Scheme 2). To achieve this goal, the emission band of UCNP should overlap with the absorption band of the chromophore. Our target compound **2** has a maximum absorption peak at 546 nm, which perfectly matches the UCL emission of $^2H_{11/2}\rightarrow{}^4I_{15/2}$ and $^4S_{3/2}\rightarrow{}^4I_{15/2}$ transitions of Er^{3+} (Fig. 1). As previously reported,[46] the addition of Hg^{2+} to the solution of as-prepared nanoprobes will cause a blue-shift of maximum absorption peak to 465 nm, forming **2'** and leading to the recovery of these UCL emission bands. Thus it is reasonable to suggest that the degree of energy transfer can be modulated by the concentration of Hg^{2+}.

UCNPs are coated with oleic acids (OA), which are hydrophobic. In order to combine the UCNP and compound **2** into one nanosystem, we employed α-cyclodextrin (α-CD) to convert the hydrophobic UCNP into the hydrophilic form (Scheme 1) by self-assembly of host (α-CD) and guest molecules (OA).[47, 48] The surface of the as-converted nanoprobes will be much easier for us to modify with compound **2**, and improve the water solubility as well.

Synthesis and Characterization of UCNP

Compound **2**, containing a thiazole electron withdrawing group and a diethylamine electron donating group, was synthesized by a two-step reactions with an overall yield of 6.3% (Scheme 3).

The OA-coated UCNPs were prepared by a modified solvothermal method.[49-55] The as-prepared UCNPs were further functionalized by attaching to α-cyclodextrin[48], followed by loading compound **2** to produce three-layer nanostructure **2**-UCNPs. Scheme 1 is a schematic illustration of UCNPs functionalized by the CD-capped OA ligands and compound **2**. The hydrophilic parts of hydroxyl groups face out-wards, rendering UCNP high water-solubility and stability.

Transmission electron microscopy (TEM) images (Fig. 2A-2D) show that there were no significant changes in size, shape and crystallinity after modification with compound **2**. These images also indicated that both OA-UCNP and **2**-UCNP had an average diameter of about 25 nm, and no evident aggregation was observed. In addition, powder X-ray diffraction (PXRD) peaks of UCNP correlated very well with the hexagonal structure of

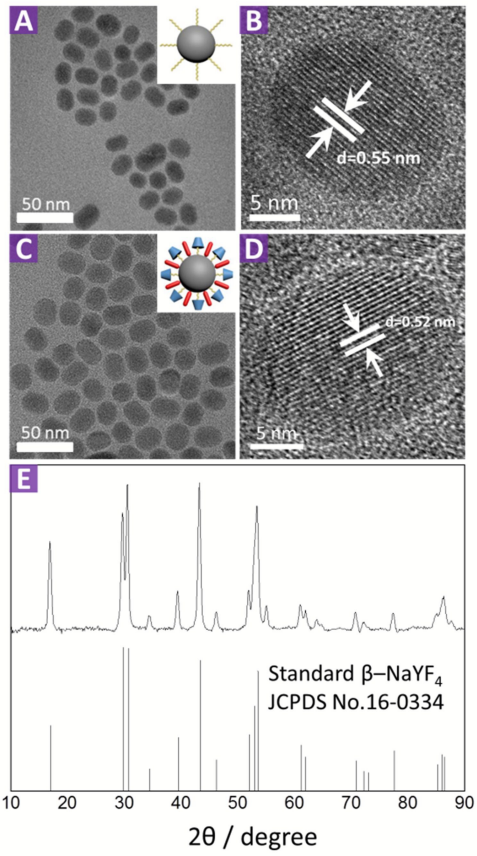

Fig. 2. TEM (A) and HR-TEM (B) images of OA-UCNP. TEM (C) and HR-TEM (D) images of **2**-UCNP. (E) XRD of UCNP ($NaYF_4$: 20% Yb, 1.8% Er, 0.5% Tm) and standard pattern of β–$NaYF_4$ (JCPDS No.16-0334).

$NaYF_4$ (Fig. 2E), and all the diffraction peaks in **2**-UCNP could be indexed to the standard pattern of β-$NaYF_4$, indicating the high purity of **2**-UCNP. This result was further confirmed by high-resolution transmission electron microscopy (HR-TEM).

The surface modification was also confirmed by Fourier transform infrared (FTIR) spectroscopy (Fig. S6). For OA-UCNP, the band at 3433 cm^{-1} is attributed to the stretching vibration of the OH group, while two peaks at 2925 and 2854 cm^{-1} belong to both symmetric and asymmetric C–H stretching vibrations, indicating the presence of OA on UCNP surface. For α-CD functionalized UCNP, the band at 1077 cm^{-1} is attributed to C–O–C stretching vibration, confirming that α-CD has attached on UCNP. Compared with OA-UCNP, **2**-UCNP showed three new peaks at 1427, 1568, 1624 cm^{-1} and one new peak at 756 cm^{-1}, which could be assigned to the C=C stretching vibration and C–H bending vibration of benzene of compound **2**, respectively. These facts indicated that compound **2** was successfully assembled on the surface of UCNP.

Sensing Properties of compound 2

In the present study, we investigated the sensing ability of compound **2** for Hg^{2+} in DMSO/HEPES (1:9, v:v). The absorption spectra of compound **2** with and without Hg^{2+} are shown in Fig. S5. In the absence of Hg^{2+}, compound **2** had a maxim

Journal Name

ARTICLE

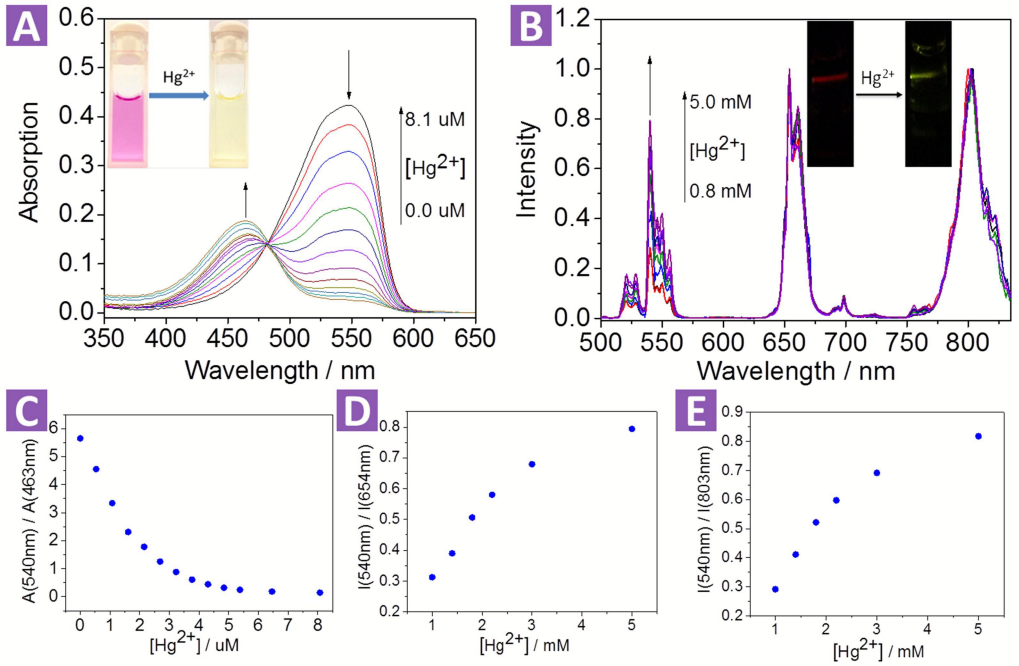

Fig. 3. (A) Absorption spectrum of 0.005 mg/mL **2**-UCNP in DMSO/HEPES (0.5:99.5, v:v) with different Hg^{2+} concentration from 0 to 8.1 uM. Inset: the photo shows the color change from red to green. (B) UCL spectrum of 1 mg/mL **2**-UCNP in DMSO with different Hg^{2+} concentration from 0.8 to 5.0 mM. Inset: the photo shows the emission change from red to green. (C) The ratio of absorption at 540 nm to 463 nm decreased when the Hg^{2+} concentration increased. (D) The ratio of UCL emission at 540 nm to 654 nm increased when the Hg^{2+} concentration increased. (E) The ratio of UCL emission at 540 nm to 803 nm increased when the Hg^{2+} concentration increased.

absorption peak at 546 nm (ε=1.51×10^5 M^{-1}·cm^{-1}). With the increase of Hg^{2+} concentration, the peak at 546 nm gradually decreased, and the absorption peak at 465 nm increased with an isosbestic point at 481 nm, leading to an evident color change from red to green. This color change is attributed to the formation of a relatively stable metal complex.[46, 56, 57] Both the sulfur atom in benzothiazolium moiety and the oxygen atom in the phenolic moiety may combine with Hg^{2+}, forcing the thiazole derivative to adopt a cis configuration, thus breaking the trans-cis dynamic equilibrium.

Sensing Properties of 2-UCNP

After the dye-loading process, the sensing property of **2**-UCNP was also investigated by both UV-Vis absorption spectrum and UCL spectrum.

For absorption spectrum, **2**-UCNP showed a broad band with the maximum absorption at 540 nm. After the addition of Hg^{2+}, the absorption peaks had a blue-shift, changing from 540 nm to 463 nm, corresponding to the color change from red to green (Fig. 3A). This blue-shift (77 nm) was in agreement with the change of the pure compound **2**, which indicated that a reaction between Hg^{2+} and the compound **2** existed at the **2**-UCNP surface. In addition, using A_{540}/A_{463} as detection sig[illegible], the limit of detection was measured to be 0.063 μM (Fig. S12).

As shown in Fig. 1, under excitation of 980 nm, the OA-UCNP showed four UCL emission bands at 514−534 nm, 534−560 nm, 635−680 nm and 775-825 nm, attributed to $^2H_{11/2}\rightarrow{}^4I_{15/2}$, $^4S_{3/2}\rightarrow{}^4I_{15/2}$ and $^4F_{9/2}\rightarrow{}^4I_{15/2}$ transitions of Er^{3+}, and $^3H_4\rightarrow{}^3H_6$ of Tm^{3+}, respectively. The dye-loaded UCNP only showed 635−680 nm and 775-825 nm emission bands, and another two bands were almost quenched through LRET process because they had overlapped with the absorption band of compound **2**.

After the addition of Hg^{2+}, the spectral overlap between the green emission band (514-560 nm) of UCNP and the absorption band (540 nm) of compound **2** was reduced, causing a decrease of LRET process, thus the emission at 514−560 nm was recovered gradually (Fig. 3B). Note that another two emission bands at 635−680 nm and 775-825 nm were not involved in the LRET process, and their intensity would not be affected before and after the addition of Hg^{2+}, which means these two bands could be used as a reference standard. Herein we employed the ratio of UCL intensity at

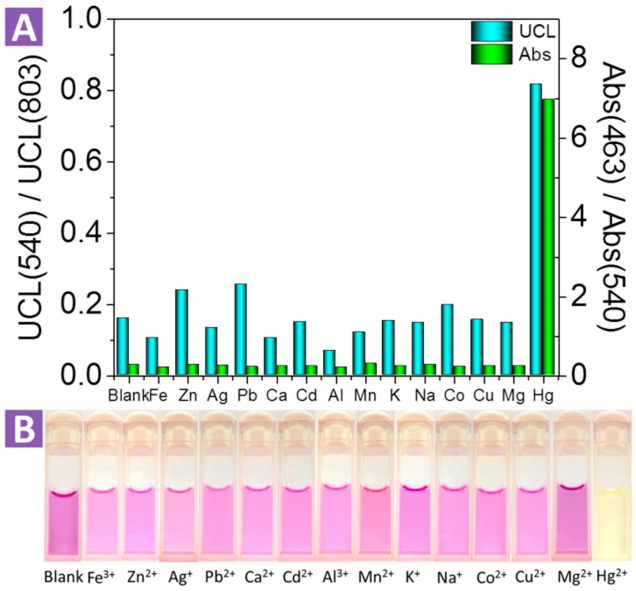

Fig. 4. (A) The blue columns correspond to the ratio of UCL emission at 540 nm to 803 nm of **2**-UCNP (1mg/ml) with Hg^{2+} and other metal ions of same concentration (3.5 mmol/L); the green columns correspond to the ratio of absorption at 463 nm to 540 nm of **2**-UCNP (0.005mg/ml) with Hg^{2+} and other metal ions of same concentration (20 μmol/L). (B) Color change of **2**-UCNP in the presence of different metal ions.

540 nm and 803 nm (I_{540}/I_{803}) as the detection signal, and the limit of detection was measured to be 0.21 μM (Fig. S13). We also chose I_{540}/I_{654} to improve the signal stability. As shown in Fig. 3D and 3E, the values of both I_{540}/I_{803} and I_{540}/I_{654} increased with the addition of Hg^{2+}.

Compared with **2**-UCNP, simply physical mixing of OA-UCNP with compound **2** did not show obvious quench of 540 nm band. For I_{540}/I_{654} and I_{540}/I_{803} values, physical mixing only led to a 4% and 8% decrease, respectively, indicating that the quench effect of **2**-UCNP was mainly ascribed to LRET process. We tested the UCL intensity change after the physical mixing and found that the 540 nm band intensity decreased very fast (Fig. S8). In 6 minutes at room temperature, the intensity will decrease about 45% (Fig. S9). These results indicated that compound **2** was easily combined with UCNP.

For an excellent ion probe, high selectivity plays a key role. To validate the selectivity of **2**-UCNP, some other metal ions such as alkali (K^+, Na^+), alkali earth (Ca^{2+}, Mg^{2+}) and some transition-metal ions (Mn^{2+}) were tested under the same condition for both absorption and emission (Fig. 4). For absorption, we calculated the absorbance ratio of 463 nm to 540 nm. Because the addition of Hg^{2+} would cause significant decrease at 540 nm and increase at 463 nm, the ratio of 463 nm to 540 nm would remarkably increase. Other metal ions do not show this effect, which led to small value of absorption ratio. For UCL spectrum, we calculated the intensity ratio of 540 nm to 803 nm. Hg^{2+} would recover the 540 nm band,

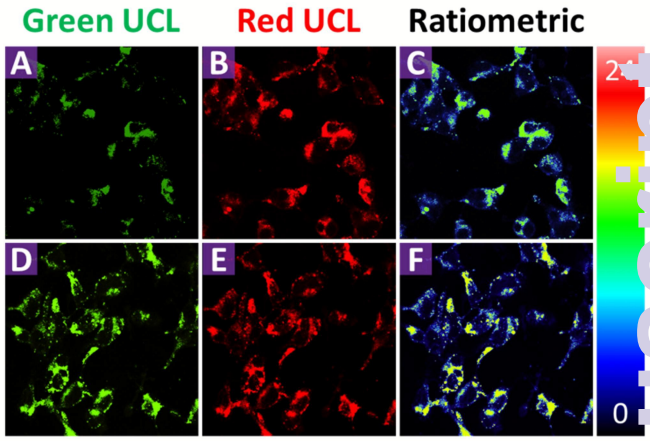

Fig. 5. Ratiometric UCL images in Hela cells (top, A to C) and 200 μM Hg^{2+} treated Hela cells (bottom, D to F) incubated with 0.5 mg/mL **2**-UCNP in 180 minutes. Emission was collected by both the green channel at 500-560 nm (A and D) and red channel at 600-700 nm (B and E). (C and F) Ratiometric UCL images with ratio of green to red channels.

increasing the ratio value, while other ions do not. Compared with absorption spectrum, the UCL intensity at 803 nm will not change, which means that the distinction between Hg^{2+} and other ions seems not as obvious as absorption spectrum. In addition, to study if the existence of other ions would interfere with the detection of Hg^{2+}, we tested the UCL intensity of **2**-UCNP containing both Hg^{2+} and other ions (Fig. S10). With or without other ions, the UCL intensity ratios only changed a little, indicating that the co-existence of other ions would not interfere with the detection of Hg^{2+}.

Furthermore, we also investigated the photo stability of **2**-UCNP under exposure of 980 nm and 365 nm light. For 980 nm exposure, after 3 hours, the absorbance of **2**-UCNP began to show slight decrease. After 9 hours, the absorbance decreased 2%. For 365 nm exposure, the absorbance decreased obviously after 1 hour and showed 27% decrease after 9 hours illumination (Fig. S11). Therefore, the nanosystem is more stable by using UCL emission as detection signal, and this significant improvement shows potential in practical applications.

Monitoring the Presence of Mercury Ion in the Living Cell

Before the application of **2**-UCNP in bioimaging, the cytotoxicity was investigated using the methyl thiazolyl tetrazolium (MTT) assay (Fig. S7). Following the incubation of **2**-UCNP for 24h, the Hela cells exhibited only minimal cytotoxicity. The cellular viability of Hela cells was still higher than 80% even at a high concentration of 800 μg/mL, indicating that the **2**-UCNP is a biocompatible nanoprobe, and it is suitable for UCL bioimaging applications.

To demonstrate the applicability of **2**-UCNP in monitoring intracellular Hg^{2+}, we conducted a laser-scanning upconversion luminescence microscopy (LSUCLM) test (Fig. 5). Both the control (Fig. 5A to 5C) and test rows (Fig. 5D to 5F) w

incubated with 0.5 mg/mL **2**-UCNP for 180 minutes, and the test row was followed by incubated with 200 μM Hg^{2+}. Under 980 nm excitation, the control row cells only showed a weak UCL emission at 540 nm, indicating the LRET process still happened in living cells. After the addition of Hg^{2+}, an enhancement of green emission was observed, which meant that the LRET process was blocked. Moreover, the intensity ofred emission almost did not change. As a result, the ratio of green to red emission showed an enhancement. These results suggested that **2**-UCNP could be used for monitoring intracellular Hg^{2+} through the ratiometric UCL method.

Conclusion

In summary, we successfully modified the surface of UCNP with compound **2** and demonstrated a new nanosystem for UCL detection and bioimaging of Hg^{2+} in living cells. The sensing mechanism was based on blocking the LRET process and recovering the green emission band after the addition of Hg^{2+}. We also employed the emission intensity ratio of 540 nm to 803 nm (I_{540}/I_{803}) as signal to confirm that the green emission band increased with the addition of Hg^{2+}. More importantly, this as-fabricated nanosystem was capable of monitoring Hg^{2+} in living cells with low cytotoxicity. This method could provide a promising strategy for further detection and bioimaging probes.

Experimental Section

Chemicals and Materials

Column chromatography was conducted over silica gel (mesh 200–300). OA, 1-octadecane (ODE 90%), 2-methylbenzo[d]thiazole, 2-bromoacetic acid, 4-(diethylamino)-2-hydroxybenzaldehyde, α-cyclodextrin and NH_4F were purchased from Sigma-Aldrich. $YCl_3{\cdot}6H_2O$ (99.9%), $YbCl_3{\cdot}6H_2O$ (99.9%), $ErCl_3{\cdot}6H_2O$(99.9%), $TmCl_3{\cdot}6H_2O$(99.9%) were purchased from Alfa Aesar. Absolute ethanol, methanol, cyclohexane, dimethyl sulfoxide and methylene chloride were of analytical grade. All of the chemicals are used without further purification.

Instrumentation

^{1}H-NMR was measured on a BrukerAV-400 spectrometer with chemical shifts reported in ppm (in CDCl3, CD_3OD or DMSO-d6; TMS as internal standard). Electrospray ionization mass spectrum (ESI-MS) was carried out on a Micromass LCTTM system. X-ray diffraction was performed on a Shimadzu XRD-6000 diffractometer at a scanning rate of 1 °/min with the 2θ range from 10 to 90° (Cu Kα radiation, λ = 1.54056 Å). HR-TEM was carried out on a JEOL JEM-2100F transmission electron microscope with an accelerating voltage of 200 kV. UV–Vis spectrum was recorded by a Shimadzu UV-2501 spectrometer. The UCL spectrum was obtained by a DM150i monochromator equipped with a R928 photon counting photomultiplier tube (PMT), in conjunction with a 980 nm diode laser. FTIR test was obtained by using a Perkin-Elmer Lambda 783 spectroscopy with KBr pellets.

Synthesis of Hg^{2+} probe

Compound **1**: 2-methylbenzo[d]thiazole (1.511 g, 10.1 mmol), 2-bromoacetic acid (2.184 g, 15.7 mmol) and 50 ml toluene were added into a one-neck flask. After refluxing for 20 hours, the solution was cooled down and the resultant precipitate was filtered and washed four times with 2 ml methanol/methylene chloride (1:9, v:v) to give a light grey solid (0.358 g): Yield 12.2%; ^{1}H NMR (400 MHz, $CDCl_3$, TMS): δ=3.18 (s, 3H, Me), 5.74 (s, 2H, NCH_2), 7.79-7.83 (m, 1H, Ph), 7.87-7.91 (m, 1H, Ph), 8.27 (d, 1H, Ph), 8.45 (d, 1H, Ph).
Compound **2**: Compound **1** (0.337 g, 1.17 mmol) and 4-(diethylamino)-2-hydroxybenzaldehyde (0.231 g, 1.20 mmol) were dissolved in 40 ml ethanol, and 40 μl piperidine was added as catalyst. After refluxing for 24 hours, the mixture was cooled down and the resulting precipitate was filtered and washed with 2 ml methylene chloride/ethyl ether (1:9, v:v) mixture for four times to produce a dark green solid (280 mg). Yield 51.7%; ^{1}H NMR (400 MHz, CD_3OD, TMS): δ=1.23 (t, 6H, Me), 3.45-3.52 (m, 4H, NCH_2), 5.24 (s, 2H, NCH_2), 6.14 (d, 1H, Ph), 6.40-6.44 (d, 1H, Ph), 7.35 (d, 1H, Ph), 7.54 (m, 2H, Ph), 7.59 (t, 1H, Ph), 7.67 (d, 1H, Ph), 8.00 (d, 1H, Ph), 8.20 (d, 1H, Ph). MS: calculated for $C_{21}H_{23}N_2O_3S^+$ 383.14, found 383.29. ESI-MS: m/z 383.29.

Synthesis of OA-UCNP

OA-UCNP was synthesized by a modified procedure according to a previous report.[49-55] $YCl_3{\cdot}6H_2O$ (235.7 mg, 0.777 mmol), $YbCl_3{\cdot}6H_2O$ (77.5 mg, 0.20 mmol), $ErCl_3{\cdot}6H_2O$ (6.9 mg, 0.018 mmol) and $TmCl_3{\cdot}6H_2O$ (1.9 mg, 0.005 mmol) were dissolved in 10 ml methanol by sonication. After removing the methanol, 6 ml oleic acid and 15 ml 1-octadecene were added. The mixture was heated up to 160°C for 30 minutes and a homogeneous solution was formed. After cooling down to room temperature, 10 ml methanol solution containing NaOH (100 mg, 2.5 mmol) and NH_4F (148 mg, 4 mmol) were added. In an Argon environment, the resulting colloidal mixture was slowly heated up to 140°C for 10 minutes to remove methanol, and then increased to 305°C, and maintained for 1.5 hours. After cooling down the solution naturally, the nanoparticles were obtained by adding ethanol, followed by centrifugation and washed with ethanol for three times.

Synthesis of an α-CD functionalized UCNP

CD-UCNP was synthesized by a modified procedure.[48] 12 ml ethanol/water (2:1, v:v) solution that contains 60 mg OA-UCNP was mixed with 12 ml α-Cyclodextrin (α-CD) aqueous solution (20 mg/ml). After vigorously stirring the mixture under room temperature, a transparent solution resulted. After stirring for 20 hours at room temperature, the solution was centrifuged (10000 rpm, 20 minutes) and the resulting particles were washed with deionized water for three times.

Synthesis of 2-UCNP

20 mg compound **2** was dissolved in 4 ml ethanol, and mixed with 10 mg α-CD functionalized UCNP. After heating at 70°C for 24 hours, the mixture was cooled down and the solution was centrifuged (9000 rpm, 10 minutes). The as-obtained particles were washed with ethanol for three times and dried in a fume hood.

Cytotoxicity Assay

To verify the cytotoxic effect of **2**-UCNP, an MTT assay was performed by treating Hela cells with 24 h incubation. Cells were passed and plated to a 70% confluence in 96-well plates, and cultured in growth medium at 37°C and 5% CO_2 for 24h. Different doses of **2**-UCNP (100, 200, 500, and 800 μg/mL) were added to the Hela cells under the same condition, followed by incubated with 5 mg/mL MTT reagent for 4h and the absorbance of each well was measured by a microplate reader (SPECTRA SLT; Labinstruments, Salzburg, Austria). Each treatment was done in six wells, and the experiments were repeated twice. Cytotoxicity was calculated relative to the absorbance of the control for each treatment. The reported percent of cell survival values were relative to untreated control cells.

Acknowledgement

Q.Z. acknowledges financial support from AcRF Tier 1 (RG 16/12 and RG133/14) and Tier 2 (ARC 20/12 and ARC 2/13) from MOE, and the CREATE program (Nanomaterials for Energy and Water Management) from NRF, Singapore. Q.Z. also thanks the support from Open Project of State Key Laboratory of Supramolecular Structure and Materials (Grant number: sklssm2015027), Jilin University, China.

Notes and references

1. Y. Yin and A. P. Alivisatos, *Nature*, 2005, **437**, 664-670.
2. H. R. Herschman, *Science*, 2003, **302**, 605-608.
3. V. Sokolova and M. Epple, *Angewandte Chemie-International Edition*, 2008, **47**, 1382-1395.
4. K.-T. Yong, I. Roy, M. T. Swihart and P. N. Prasad, *Journal of Materials Chemistry*, 2009, **19**, 4655-4672.
5. Y. Wang, Z. Chen, Y. Liu and J. Li, *Nanoscale*, 2013, **5**, 7349-7355.
6. Z. Wang, Z. Yan, N. Sun and Y. Liu, *Biosensors and Bioelectronics*, 2015, **68**, 771-776.
7. Y. Wang, K. Qu, L. Tang, Z. Li, E. Moore, X. Zeng, Y. Liu and J. Li, *TrAC Trends in Analytical Chemistry*, 2014, **58**, 54-70.
8. X. Chen, Y. Wang, Y. Zhang, Z. Chen, Y. Liu, Z. Li and J. Li, *Analytical Chemistry*, 2014, **86**, 4278-4286.
9. J.-C. G. Buenzli, *Chemical Reviews*, 2010, **110**, 2729-2755.
10. A. Y. Louie, *Chemical Reviews*, 2010, **110**, 3146-3195.
11. Q. Ju, D. Tu, Y. Liu, H. Zhu and X. Chen, *Combinatorial Chemistry & High Throughput Screening*, 2012, **15**, 580-594.
12. K. E. Sapsford, W. R. Algar, L. Berti, K. B. Gemmill, B. J. Casey, E. Oh, M. H. Stewart and I. L. Medintz, *Chemical Reviews*, 2013, **113**, 1904-2074.
13. M. S. T. Gonçalves, *Chemical Reviews*, 2009, **109**, 190-212.
14. Y. Xing and J. Rao, *Cancer Biomarkers*, 2008, **4**, 307-319.
15. E. Downing, L. Hesselink, J. Ralston and R. Macfarlane, *Science*, 1996, **273**, 1185-1189.
16. F. Wang and X. Liu, *Journal of the American Chemical Society*, 2008, **130**, 5642-+.
17. F. Wang, X. Xue and X. Liu, *Angewandte Chemie-International Edition*, 2008, **47**, 906-909.
18. F. Auzel, *Chemical Reviews*, 2004, **104**, 139-174.
19. J. Zhou, Z. Liu and F. Y. Li, *Chemical Society Reviews*, 2012, **41**, 1323-1349.
20. M. Haase and H. Schäfer, *Angewandte Chemie International Edition*, 2011, **50**, 5808-5829.
21. M. Yu, F. Li, Z. Chen, H. Hu, C. Zhan, H. Yang and C. Huang, *Analytical Chemistry*, 2009, **81**, 930-935.
22. H. Zijlmans, J. Bonnet, J. Burton, K. Kardos, T. Vail, R. . Niedbala and H. J. Tanke, *Analytical Biochemistry*, 1999, **267**, 30-36.
23. L. Xiong, Z. Chen, Q. Tian, T. Cao, C. Xu and F. Li, *Analytical Chemistry*, 2009, **81**, 8687-8694.
24. F. Wang, Y. Han, C. S. Lim, Y. Lu, J. Wang, J. Xu, H. Chen, C. Zhang, M. Hong and X. Liu, *Nature*, 2010, **463**, 1061-1065.
25. J. Zhou, Y. Sun, X. Du, L. Xiong, H. Hu and F. Li, *Biomaterials*, 2010, **31**, 3287-3295.
26. N. M. Idris, Z. Li, L. Ye, E. K. Wei Sim, R. Mahendran, P. C.-L. Ho and Y. Zhang, *Biomaterials*, 2009, **30**, 5104-5113.
27. Z. Zhou, H. Hu, H. Yang, T. Yi, K. Huang, M. Yu, F. Li and C. Huang, *Chemical Communications*, 2008, DOI: 10.1039/b809021a, 4786-4788.
28. Z. Chen, H. Chen, H. Hu, M. Yu, F. Li, Q. Zhang, Z. Zhou, T. Yi and C. Huang, *Journal of the American Chemical Society*, 2008, **130**, 3023-3029.
29. Y. I. Park, K. T. Lee, Y. D. Suh and T. Hyeon, *Chemical Society Reviews*, 2015, **44**, 1302-1317.
30. Y. Zhou, W. Chen, J. Zhu, W. Pei, C. Wang, L. Huang, C. Yao, Q. Yan, W. Huang, J. S. C. Loo and Q. Zhang, *Small*, 2014, **10**, 4874-4885.
31. C. Wang, L. Cheng and Z. Liu, *Biomaterials*, 2011, **32**, 1110-1120.
32. J.-C. Zhou, Z.-L. Yang, W. Dong, R.-J. Tang, L.-D. Sun and C.-H. Yan, *Biomaterials*, 2011, **32**, 9059-9067.
33. L. Xiong, T. Yang, Y. Yang, C. Xu and F. Li, *Biomaterials*, 2010, **31**, 7078-7085.
34. H. Hu, M. Yu, F. Li, Z. Chen, X. Gao, L. Xiong and C. Huang, *Chemistry of Materials*, 2008, **20**, 7003-7009.
35. Y. Liu, M. Chen, T. Cao, Y. Sun, C. Li, Q. Liu, T. Yang, L. Yao, W. Feng and F. Li, *Journal of the American Chemical Society*, 2013, **135**, 9869-9876.
36. R. Deng, X. Xie, M. Vendrell, Y.-T. Chang and X. Liu, *Journal of the American Chemical Society*, 2011, **133**, 20168-20171.
37. J. Peng, W. Xu, C. L. Teoh, S. Han, B. Kim, A. Samanta, J. C. Er, L. Wang, L. Yuan, X. Liu and Y.-T. Chang, *Journal of the American Chemical Society*, 2015, **137**, 2336-2342.
38. Y. Liu, S. Zhou, D. Tu, Z. Chen, M. Huang, H. Zhu, E. Ma and X. Chen, *Journal of the American Chemical Society*, 2012, **134**, 15083-15090.
39. Z. Li, S. Lv, Y. Wang, S. Chen and Z. Liu, *Journal of the American Chemical Society*, 2015, **137**, 3421-3427.

40. Y. Xiao, L. Zeng, T. Xia, Z. Wu and Z. Liu, *Angewandte Chemie International Edition*, 2015, **54**, 5323-5327.
41. Z. W. Chen, Z. Liu, Z. H. Li, E. G. Ju, N. Gao, L. Zhou, J. S. Ren and X. G. Qu, *Biomaterials*, 2015, **39**, 15-22.
42. Y. Zhou, W. Pei, X. Zhang, W. Chen, J. Wu, C. Yao, L. Huang, H. Zhang, W. Huang, J. S. Chye Loo and Q. Zhang, *Biomaterials*, 2015, **54**, 34-43.
43. Y. Zhou, W. Pei, C. Wang, J. Zhu, J. Wu, Q. Yan, L. Huang, W. Huang, C. Yao, J. S. C. Loo and Q. Zhang, *Small*, 2014, **10**, 3560-3567.
44. Z. Guo, W. Zhu, M. Zhu, X. Wu and H. Tian, *Chemistry – A European Journal*, 2010, **16**, 14424-14432.
45. K. W. Kramer, D. Biner, G. Frei, H. U. Gudel, M. P. Hehlen and S. R. Luthi, *Chemistry of Materials*, 2004, **16**, 1244-1251.
46. S. Tatay, P. Gaviña, E. Coronado and E. Palomares, *Organic Letters*, 2006, **8**, 3857-3860.
47. Q. Liu, M. Chen, Y. Sun, G. Chen, T. Yang, Y. Gao, X. Zhang and F. Li, *Biomaterials*, 2011, **32**, 8243-8253.
48. Y. Wang, J. F. Wong, X. Teng, X. Z. Lin and H. Yang, *Nano Letters*, 2003, **3**, 1555-1559.
49. Z. Li, Y. Zhang and S. Jiang, *Advanced Materials*, 2008, **20**, 4765-4769.
50. H.-X. Mai, Y.-W. Zhang, R. Si, Z.-G. Yan, L.-d. Sun, L.-P. You and C.-H. Yan, *Journal of the American Chemical Society*, 2006, **128**, 6426-6436.
51. X. Wang, J. Zhuang, Q. Peng and Y. Li, *Nature*, 2005, **437**, 121-124.
52. Q. Liu, W. Feng, T. Yang, T. Yi and F. Li, *Nature Protocols*, 2013, **8**, 2033-2044.
53. F. Wang, R. Deng and X. Liu, *Nature Protocols*, 2014, **9**, 1634-1644.
54. C. Li, Z. Quan, J. Yang, P. Yang and J. Lin, *Inorganic Chemistry*, 2007, **46**, 6329-6337.
55. H.-S. Qian and Y. Zhang, *Langmuir*, 2008, **24**, 12123-12125.
56. J. T. C. Wojtyk, P. M. Kazmaier and E. Buncel, *Chemistry of Materials*, 2001, **13**, 2547-2551.
57. O. A. Fedorova, Y. V. Fedorov, A. I. Vedernikov, S. P. Gromov, O. V. Yescheulova, M. V. Alfimov, M. Woerner, S. Bossmann, A. Braun and J. Saltiel, *The Journal of Physical Chemistry A*, 2002, **106**, 6213-6222.